Journal of Molecular Catalysis A: Chemical 319 (2010) 92–97

Contents lists available at ScienceDirect

Journal of Molecular Catalysis A: Chemical

journal homepage: www.elsevier.com/locate/molcata

Low temperature CO oxidation over gold supported mesoporous Fe–TiO_2

K.M. Parida[a,*], Nruparaj Sahu[a], P. Mohapatra[b], M.S. Scurrell[c]

[a] Colloids and Materials Chemistry Department, Institute of Minerals and Materials Technology (CSIR), Bhubaneswar 751013, Orissa, India
[b] Dalmia Institute of Scientific and Industrial Research (DISIR), Rajgangpur 770017, Orissa, India
[c] Molecular Sciences Institute, School of Chemistry, University of the Witwatersrand, Johannesburg 2050, South Africa

ARTICLE INFO

Article history:
Received 3 November 2009
Received in revised form 9 December 2009
Accepted 11 December 2009
Available online 22 December 2009

Keywords:
Gold/titania
Iron
Oxygen vacancy
New adsorption site

ABSTRACT

A series of gold supported mesoporous Fe–TiO_2 samples were prepared by the borohydrate reduction method. Fe–TiO_2 (1.0, 3.0, 5.0, 7.0 wt%) was prepared by the incipient wetness impregnation method. These catalysts were characterized by TEM, XPS, UV–vis DRS, photoluminescent spectra (PL), TPR/TPD, BET surface area etc. A detail study has been carried out to know the effect of iron on the physico-chemical and catalytic property of gold–titania catalyst. Iron doping influences the surface and electronic properties of Au–TiO_2. The activity of these catalysts for CO oxidation was evaluated. We observed higher catalytic activity of gold supported Fe–TiO_2 catalysts compared to gold supported TiO_2. We found that the catalyst with 5 wt% of Iron was the most active catalyst. The gold supported Fe–TiO_2 catalyst does not lose its activity over several hours even at 500 °C, in marked contrast to Au–TiO_2. Iron doping enhances the catalytic activity of Au–TiO_2 as well as stabilizes the catalyst at high temperature.

1. Introduction

Supported gold nanoparticles were reported to be very active in a wide variety of chemical reactions like oxidation of carbon monoxide and hydrocarbons, hydrogenation of carbon oxides and reduction of nitric oxide. Among these, CO oxidation over oxides supported gold nanoparticle has been most extensively investigated [1,2]. The low temperature CO oxidation process has several applications such as air purification, elimination of CO from automobile exhaust, water gas shift reaction and fuel cells. Although supported gold catalysts are active for low temperature CO oxidation, problems are found with the stability of the gold nanoparticles against temperature and other reaction conditions. Gold nanocluster catalysts are known to deactivate with reaction time [3–5]. Many studies have been performed to stabilize the supported gold nanoparticles and improve the catalytic activity at ambient temperature. It has been found that the use of binary mixed oxides as gold supports could provide a good solution for the stabilization of gold nanoparticles. The gold particles can be anchored to the support, which stabilizes them and prevents their sintering [6,7]. Qian et al. modified the surface of SiO_2 with a small amount of highly dispersed CoO_x and successfully synthesized highly active Au–Co*O*x–SiO_2 catalyst, demonstrating excellent catalytic activity in low temperature CO oxidation [8]. Chimentao et al. reported the gold–copper alloy catalysts, prepared by impregnation of TiO_2 support and tested in the gas-phase epoxidation of propene. They found that copper content in the catalyst contributed to an increase in activity and selectivity to propene oxide [9]. Not all the additives showed the positive effect to the supported gold catalyst. Ma et al. reported that CuO, ZnO, NiO, CaO, Ga_2O_3, ZrO_2 and rare earths additives to gold–titania catalyst are beneficial to the reaction for CO oxidation, whereas MoO_3 or WO_3 produce a negative effect on gold stability [10]. Debeila et al. found that doping of In_2O_3 to gold titania lowered the catalytic activity but increased the resistance to sintering [11], whereas Gonzalez et al. reported that Au–In_2O_3–TiO_2 catalyst is highly active and resistant to sintering [12].

Iron-containing catalysts are also active for CO oxidation [13–17]. Gold and iron supported on Y-type zeolite is highly active for carbon monoxide oxidation [18]. Guczi et al. investigated the FeO*x*–Au–SiO_2–Si (1 0 0) model catalyst and found that gold promoted the catalytic activity of FeO_x for CO oxidation [19]. Carriazo et al. studied gold supported on Fe, Ce, and Al pillared bentonites for CO oxidation reaction [20]. Recently Wu et al. studied the photocatalytic activity of the Au–Fe–TiO_2 and found that it exhibited excellent visible light and UV-light activity. They reported that the synergistic effects of Fe^{3+} and Au were responsible for improving the photocatalytic activity [21]. Shou et al. found that loading a large amount of FeO_x, for CO oxidation in excess H_2, enhances the catalytic activity of 1 wt% Au–TiO_2 catalyst [22]. Carrettin et al. reported that, addition of iron to gold supported TiO_2 (Degussa P25) increases the number of oxygen defect sites that activate oxygen to

* Corresponding author at: Colloids and Materials Chemistry Department, Institute of Minerals and Materials Technology (CSIR), Bhubaneswar 751013, Orissa, India. Tel.: +91 674 2581636 425; fax: +91 674 2581637.
E-mail address: paridakulamani@yahoo.com (K.M. Parida).

1381-1169/$ – see front matter © 2009 Elsevier B.V. All rights reserved.
doi:10.1016/j.molcata.2009.12.005

form peroxide and superoxide species, which is responsible for the better activity of the catalyst [23]. Albonetti et al. had prepared a series of gold/iron clusters on titania support from bimetallic carbonyl clusters and characterized to determine how the nature of the precursors and the thermal treatment conditions affected the dispersion of the active phase and the catalytic activity for the decomposition of toluene [24].

In the present paper a detail study have been carried out on the synthesis of gold supported Fe–TiO_2 catalysts, its characterization and CO oxidation. The emphasis in this study is to prepare highly stable and durable supported gold catalysts.

2. Experimental

2.1. Preparation of titania

Titania was prepared by a sol–gel method using titanium isopropoxide as the titania precursor at pH = 3. A measured amount of titanium(IV) isopropoxide was placed in a beaker and 8 times its volume of propan-2-ol added to it. This mixture was placed in an ice bath with vigorous stirring and deionised water (preadjusted to pH 3 using dilute nitric acid) added to it dropwise. After complete precipitation, the gel formed was refluxed at 80 °C for 10 h, allowed to cool, filtered and then dried at 100 °C for 12 h.

2.2. Preparation of iron-doped titania

Iron-doped titania with various wt% (1.0, 3.0, 5.0, 7.0) of iron was prepared by an aqueous incipient wetness impregnation method using ferric nitrate as the iron source. The suspended mass was evaporated to dryness on a hot plate while stirring and dried in an oven at 120 °C. The prepared samples were calcined at 400 °C using a heating rate of 10 °C/min in a muffle furnace and held at the upper temperature for 4 h. These samples are denoted as *x*Fe–TiO_2 (where x (1, 3, 5 & 7) wt% of iron in the sample).

2.3. Preparation of gold supported iron titania

Gold (1 wt%) supported on iron–titania (*x*Fe–TiO_2) samples were prepared by the borohydrate reduction method. The supports were suspended in deionised water and the required amount of dilute $HAuCl_4$ (0.01 mol dm^{-3}) added dropwise with continuous stirring. After 2 h of addition, the pH was raised to 8.5 using 15% NH_4OH and the mixture aged for 2 h. A solution of $NaBH_4$, freshly prepared in deionised ice-water, was added to the mixture. The suspension was then filtered, washed several times with warm deionised water and dried overnight at 120 °C for 12 h. These samples are denoted with prefix Au (for example the sample with 5 wt% Fe was denoted as Au–5Fe–TiO_2). For comparison purpose gold supported iron-P25 titania (Degussa, Germany) catalyst was prepared.

2.4. Physicochemical characterization

Specific surface areas (BET) of the catalysts were measured by the N_2 adsorption–desorption method at liquid nitrogen temperature (−196 °C) using an ASAP 2020 (Micromeritics, USA). Prior to the analysis, samples were degassed at 200 °C for 4 h. UV–vis DRS spectra was recorded in a UV–vis spectrophotometer (Varian, Australia). The spectra were recorded in the range of 200–800 nm using boric acid as the reference standard. Fluorescence measurements were carried out with a Hitachi F-4500 spectrofluorometer with a 150 W xenon lamp as the light source under photoexcitation at 380 nm. TPR/TPD was performed using CHEMBET-3000 (Quantachrome, USA) instrument in the temperature range of 40–800 °C. About 0.1 g of powdered sample was contained in a quartz "U" tube and degassed at 250 °C for 1 h with ultra pure nitrogen gas. After cooling the sample to room temperature, for TPR, H_2 (10%H_2 balanced with argon) gas was flowed through the sample maintaining a heating rate of 10 °C/min to record the profile. For O_2-TPD, 5% O_2 gas was flowed for 1 h and profile was recorded in continuous flow of nitrogen. Surface morphology was studied by Transmission Electron Microscopy (FEI, TECNAI G2 20, TWIN) operating at 200 kV. The samples for electron microscopy were prepared by dispersing the powder in ethanol and coating the very dilute suspension on carbon coated Cu grids. TEM images were recorded by using Gatan CCD camera. The particle sizes were determined by using several TEM micrographs and the IMAGEJ analysis package. XPS spectra were recorded on a VG Microtech Multilab ESCA 3000 spectrometer that was equipped with an Al K X-ray source ($h\nu$ = 1486.6 eV). Binding energy calibration was performed with C 1s core level at 284.6 eV.

2.5. Catalytic activity evaluation

The activities of the catalyst samples in the oxidation of carbon monoxide were measured using a fixed-bed flow reactor. About 150 mg of catalyst was diluted with 300 mg of quartz and placed in the reactor. This was pretreated in situ for 1 h at 300 °C with 5% O_2 and balances helium at a flow rate of 40 ml min^{-1} and then allowed to cool to room temperature. The reactant gas mixture consisting of 10% CO, 5% O_2 and 85% He at a flow rate of 25 ml min^{-1} was passed through the reactor and the effluent gases from the reactor were analyzed using on-line gas chromatography.

3. Results and discussion

3.1. Characterization

The N_2 adsorption–desorption isotherms of Au–TiO_2, Au–1Fe–TiO_2, Au–5Fe–TiO_2 and Au–7Fe–TiO_2 samples are shown in Fig. 1. A type IV isotherm and an H1 hysteresis loop clearly indicate the mesoporous nature of the TiO_2. Pore volume (single point total pore volume of pores at P/P_o = 0.99) and pore size (determined from BJH adsorption branch of the isotherm) of the samples are given in Table 1. On increasing the activation temperature of the TiO_2, pore volume decreases and pore size increases. This may be due to the collapse of mesoporous structure upon calcination, which results in the shifting of pore size to a larger mesoporous region. The BET specific surface area of iron-doped titania samples calcined at 400 °C are relatively high

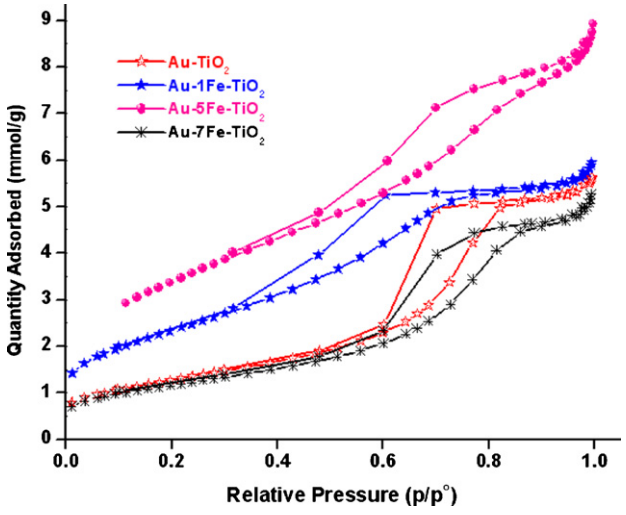

Fig. 1. Nitrogen adsorption–desorption isotherms of Au–TiO_2, Au–1Fe–TiO_2, Au–5Fe–TiO_2 and Au–7Fe–TiO_2 samples.

Table 1
Textural properties of TiO_2, Au–TiO_2 and Au–x Fe–TiO_2 samples.

Catalyst	BET surface area (m^2/g)	Pore volume (cm^3/g)	Pore size (nm)
TiO_2 (as synthesized, 120 °C)	625.7	0.58	2.06
TiO_2 (400 °C)	59.0	0.13	3.6
Au–TiO_2 (400 °C)	58.0	0.18	5.6
Au–1Fe–TiO_2 (400 °C)	198.9	0.21	4.2
Au–5Fe–TiO_2 (400 °C)	272.4	0.31	4.7
Au–7Fe–TiO_2 (400 °C)	93.6	0.18	6.9

compared with the undoped sample, confirms the frameworks of mesoporous Au–x Fe–TiO_2 have better thermal stability than TiO_2. We assumed that, this may be due to the formation of iron titania composite oxides, which effectively stabilized surface area of TiO_2. However there is a decrease in specific surface area with higher iron loading, may be due to the blockage of pores by excess iron. The pore size distribution measurement indicates that the Au–x Fe–TiO_2 sample have pronounced mesoporosity of a narrow pore size distribution. Large surface area and 3D-connected pore system play an important role in catalyst design for its ability to improve the molecular transport of reactants and products.

UV–vis DRS spectra (Fig. 2) demonstrate a significantly enhanced absorption of gold nanoparticles in the visible range at 500–600 nm due to plasmon resonance. The absorption of Au–TiO_2, Au–1Fe–TiO_2 and Au–5Fe–TiO_2 was found to be at 572, 590 and 580 nm respectively. Surface plasmon resonance of metallic nanoparticles depends on the particle size, shape, loading and surrounding environment. The red shift of plasmon band of Au–x Fe–TiO_2 would be attributed to the different environment surrounding the Au particles compared with that existing in the iron-free Au–TiO_2. There may be interactions between the Au particles and the Fe–TiO_2 support [21]. Strong absorption at 200–340 nm is characteristic of the TiO_2.

PL spectra of doped and undoped TiO_2 exhibited luminescence peak at 570 nm under photoexcitation at 380 nm (Fig. 3). The physical origin of the PL may be due to the radiative recombination of self-trapped excitons localized within TiO_6 octahedra and oxygen vacancies [25,26]. PL intensity of titania was found to decrease by gold and/or iron doping. This degree of quenching could be related to the quantity of surface-active sites or oxygen vacancies [27]. Modified titania showing larger quenching in the photoluminescence is supposed to have higher quantity of surface-active

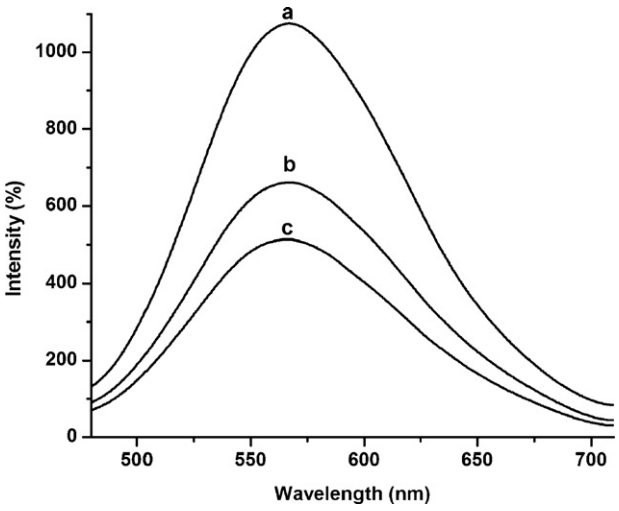

Fig. 3. PL spectra of (a) TiO_2, (b) Au–TiO_2, and (c) Au–5Fe–TiO_2.

sites. Iron doping generates oxygen vacancies (point defects) on metal-oxide supports, which play an important role as metal cluster nucleation sites. Theoretical studies have shown that electron transfer from defects to the Au cluster facilitates CO oxidation [28].

The temperature-programmed reduction (TPR) profile of Au–TiO_2 and Au–5Fe–TiO_2 samples are given in Fig. 4. Generally titania is reluctant to reduce even at higher temperatures. Reduction temperature in presence of hydrogen is reported at 1300 °C [29]. In our experimental condition it is partially reduced to TiO_{2-x} by hydrogen and this process is promoted by the presence of dispersed metal crystallites. So the only peak in case of Au–TiO_2 at 420 °C has been assigned to partial reduction of Ti^{4+} to Ti^{3+}. This indicates that presence of gold facilitates the reduction of Ti^{4+} species [30,31]. The partial reduction of Ti^{4+} was found to be at lower temperature in case of Au–5Fe–TiO_2. The shoulder peak at 330 °C, corresponds to the dehydroxylation of the TiO_2 surface and also partial reduction of Ti^{4+} to Ti^{3+}. Thus iron doping strongly facilitates the reduction of Ti^{4+} in case of Au–5Fe–TiO_2. This suggests that there is strong interaction between metal and support. Peak at 150 °C was assigned to reduction of hydroxylated Fe_2O_3 to Fe_3O_4 (magnetite). Peaks at 480 °C and 580 °C correspond to the reduction temperatures of the Fe^{3+} and Fe^{2+} states of iron [32,33]. According to the literature, three main reduction peaks was observed for

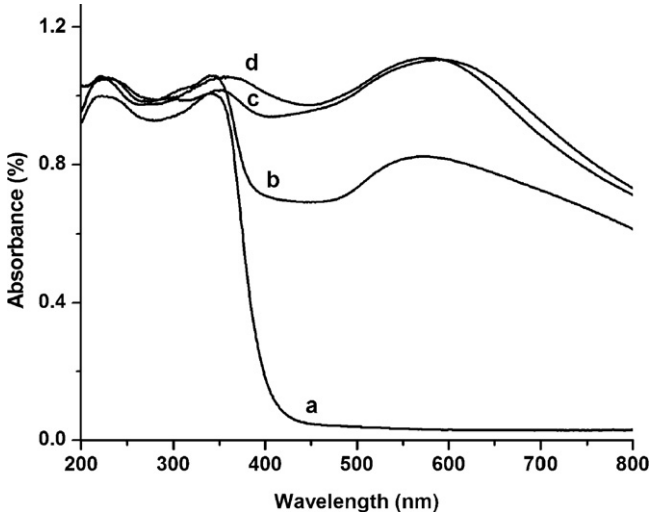

Fig. 2. UV–vis DRS of (a) TiO_2, (b) Au–TiO_2, (c) Au–1Fe–TiO_2, and (d) Au–5Fe–TiO_2.

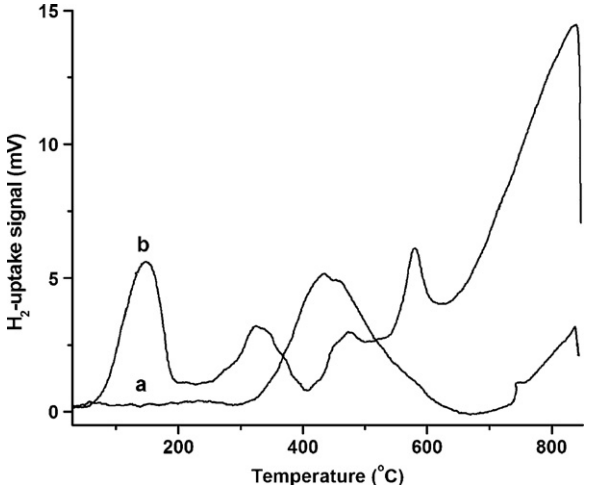

Fig. 4. H_2-TPR profile of (a) Au–TiO_2 and (b) Au–5Fe–TiO_2.

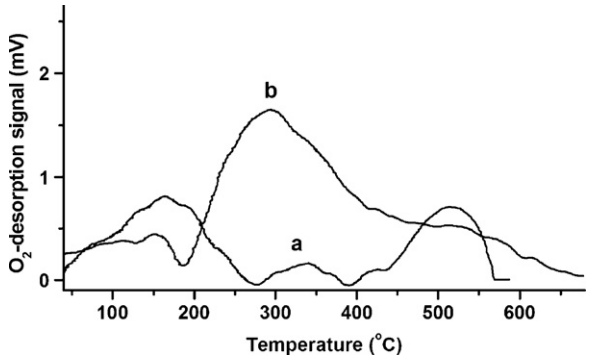

Fig. 5. O_2-TPD profile of (a) Au–TiO_2 and (b) Au–5Fe–TiO_2.

gold/iron oxide samples with the two peaks at 150 °C and 230 °C being attributed to the reduction of hydroxylated and nonhydroxylated Fe_2O_3 respectively to Fe_3O_4 (magnetite). This reduction of Fe_2O_3 to Fe_3O_4 occurs at a much lower temperature compared to that of the pure iron oxide on which this transformation has been observed at 390 °C and 450 °C [34–36]. This indicates that the presence of gold strongly facilitates the reduction of Fe_2O_3 species. No reduction peak for gold was found and hence it is present in zero oxidation state.

The temperature-programmed desorption (O_2-TPD) profiles of O_2 adsorbed over Au–TiO_2 and Au–5Fe–TiO_2 samples are given in Fig. 5. Peak at 160 °C may be attributed to the O_2 molecules physically adsorbed on external surface and we assumed that the peak at 525 °C is due to the desorption of chemisorbed O_2 molecules in the pores of catalysts. A highly intense new desorption peak at 300 °C was observed in case of Au–5Fe–TiO_2. This may be attributed to the adsorption of O_2 at metal support interfacial sites. Thus TPD results reveal that the doping of iron gives rise to certain new adsorption sites at Au–TiO_2 interfaces for the adsorption and activation of O_2 molecules.

From TEM images (Figs. 6 and 7), it was observed that gold nanoparticles were uniformly distributed over the TiO_2 surface, with the existence of gold in the samples being confirmed by energy dispersive X-ray spectroscopy (EDX) measurement. In the selected

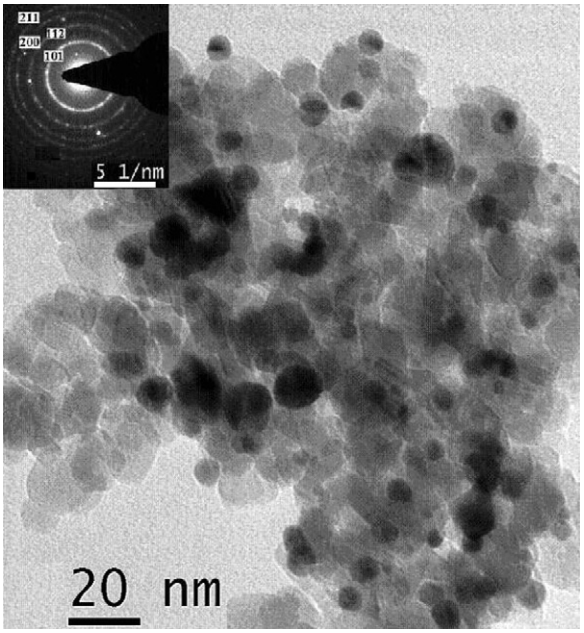

Fig. 6. TEM image of Au–TiO_2 (inset is SAED).

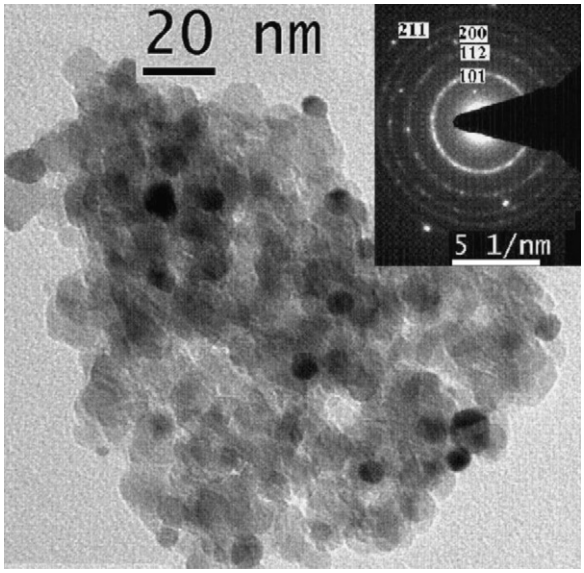

Fig. 7. TEM image of Au–5Fe–TiO_2 (inset is SAED).

area electron diffraction (SAED) pattern (inset in figures), the concentric diffraction rings clearly reveal the presence of the {1 0 1}, {1 1 2}, {2 0 0}, and {2 1 1} planes of anatase TiO_2, indicating the highly crystalline nature of samples.

There is a decrease in the particle size of gold on iron doping. The particle size distribution graph is well fitted by a Gaussian function and the nanocrystallite size distribution of both Au–TiO_2 and Au–5Fe–TiO_2 samples were found to be narrow one with an average particle size of 10.0 and 7.6 nm with a standard deviation of 2.6 and 1.5 nm respectively.

Gold particles are highly dispersed on the surface of the TiO_2. These particles are attached to the surface of the TiO_2 by their {1 1 1} plane, which comprises the flat surface. These contact surfaces provide the longest area around the perimeter interface of the gold particle (Fig. 8). High-resolution lattice image confirmed that the samples were oriented mostly in one direction, corresponding to the {1 0 1} interplaner spacing of anatase TiO_2. A set

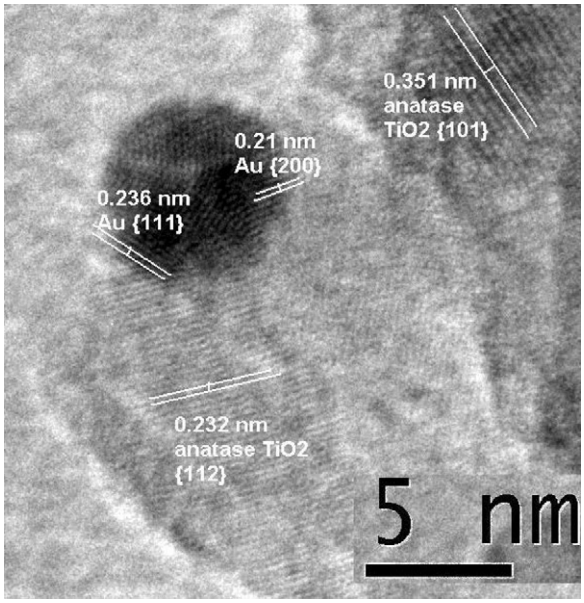

Fig. 8. HRTEM of Au–TiO_2.

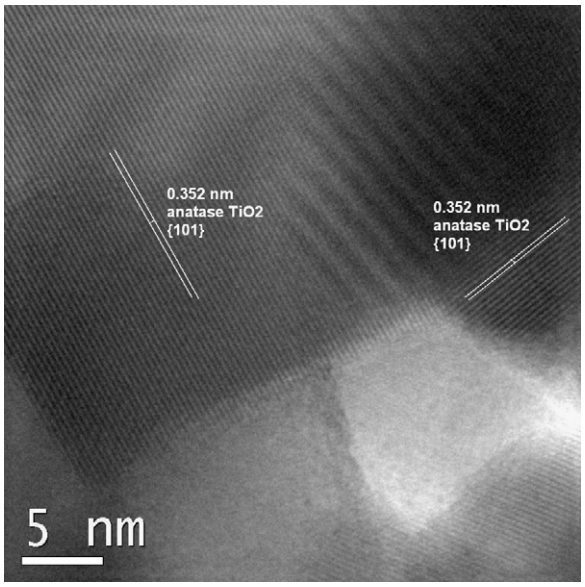

Fig. 9. Au–TiO_2 Moire.

of {1 0 1} plane is superimposed to the other set of {1 0 1} planes. Interference between the two sets (Moire patterns) is clearly seen (Fig. 9).

Particle size of gold is strongly influenced by the temperature. The particle size of Au in case of Au–TiO_2 at 500 °C is drastically increased (mean particle size was found to be 24 nm) and found to be non-uniform. But in case of Au–5Fe–TiO_2 even at 500 °C it is found to be stable (8 nm). The effect on the stability of small metal particles by additives may be due to the creation of surface defects. Certain modified or mixed metal oxides may have surface defects that hinder the movement of metal particles. For an example, in case of Au/IrO_2/TiO_2, in which IrO_2 islands sit on top of TiO_2 surface, and Au particles sit on top of IrO_2 islands, so the migration of gold to an adjacent gold particle is hindered by the large energy barrier across the TiO_2 surface [6,7].

The O 1s binding energies was found to be at 529.6 eV, which is assigned to bulk oxide (O^{2-}) in the TiO_2 lattice. The binding energy of Ti 2p is 458.2 and 458.4 eV for Au–TiO_2 and Au–5Fe–TiO_2 respectively. The peak ratio of Ti $2p_{3/2}$ and Ti $2p_{1/2}$ is equal to 0.5 and the BE difference, BE = BE (Ti $2p_{1/2}$) − BE (Ti $2p_{3/2}$), was always 5.7 eV for Ti^{4+}. BE of Ti 2p of Au–5Fe–TiO_2 catalysts showed a slightly higher binding energy as compared to the Au–TiO_2. The XPS peak of iron was found to be at 710.7 eV, indicating the presence of Fe in the +3 oxidation state. The oxidation state of Au also plays an important role in the oxidation reaction. The binding energy for bulk metallic gold is 84.0 eV and oxidized Au species is around 85.5 (Au^+) and 86.3 eV (Au^{3+}) as reported in the literature [37]. The binding energy of Au $4f_{7/2}$ was found at 84.3 and 83.8 eV for Au–TiO_2 and Au–5Fe–TiO_2 respectively (Table 2). The BE of Au 4f for Au–5Fe–TiO_2 is found to be lower by 0.5 eV while the BE of Ti 2p showed a slightly higher than Au–TiO_2. It can be concluded that there may exist strong interactions between Au and the support, which may change the electronic property of Au–5Fe–TiO_2 [21]. This result is in good agreement with the observed red shift in the plasmon band of Au–5Fe–TiO_2.

Table 2
Binding energy (eV) of Au–TiO_2 and Au–5Fe–TiO_2 samples.

Sample	Au $4f_{7/2}$	Ti $2p_{3/2}$	O 1s	Fe $2p_{3/2}$
Au–TiO_2	84.3	458.2	529.47	–
Au–5Fe–TiO_2	83.8	558.4	529.6	710.7

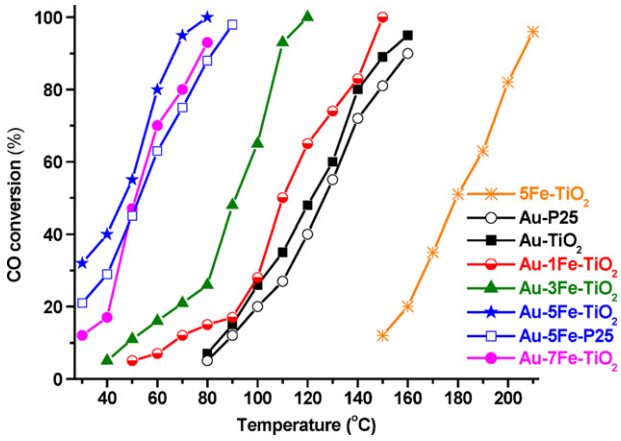

Fig. 10. Activity of catalysts for CO oxidation as a function of temperature.

3.2. CO oxidation

There is a dramatic increase in the catalytic activity towards CO oxidation for gold supported *x*Fe–TiO_2 series of catalysts compared to Au–TiO_2 and *x*Fe–TiO_2 catalyst. We found that *x*Fe–TiO_2 catalyst is inactive up to 150 °C. TiO_2 prepared by sol gel method in the present work was found to be better active than P25-TiO_2 as support. So a detailed study has been carried out with the TiO_2 prepared by sol gel method. It was observed that for Au–TiO_2 catalyst, CO oxidation starts at 80 °C, whereas the Au–*x*Fe–TiO_2 samples were active at room temperature. For Au–TiO_2 catalyst there is only 7% conversion at 80 °C whereas the Au–5Fe–TiO_2 sample achieves 100% conversion at same temperature. We observed > 14 fold higher activity for gold supported *x*Fe–TiO_2 series of catalysts compared to Au–TiO_2 catalysts. It was found that on increasing the iron doping, catalytic activity increases up to 5 wt% and then decreases (Fig. 10). From the above results we assumed that, the optimum doping amount for the gold supported Fe–TiO_2 series of samples was 5 wt%, and further detailed study has been carried out in this sample.

The inclusion of iron had a beneficial effect on the stability of the catalysts. Moreau and Bond [38,39] reported that the Au–FeO*x*–TiO_2 remained perfectly stable for 50 h. They are of the opinion that the gold particles are in contact with an iron-containing phase (such as FeO(OH)), and inclusion of iron form oxygen vacancies at which oxygen molecule can chemisorbed, which is responsible for the better stability and activity of the catalyst. The negative effect of calcination, which converts FeO(OH) to Fe_2O_3, was also highlighted in the paper. Freshly precipitated hydroxides have previously been recommended as supports [40], and recent work [41] shows that co-precipitated Au–FeO_x catalysts maintain their activity at room temperature.

Au–FeO*x*-oxide catalysts have consequently two sorts of catalytic component: (i) gold deposited on the principal oxide, probably still suffering from deactivation due to carbonate formation and (ii) gold deposited on possibly FeO(OH), which is clearly responsible for the high activity and stability. The relative contributions of these two functions will depend on the iron loading and on the specific surface area of the support.

It was also found that the iron-doped, gold-modified titania catalyst does not deactivate over several hours on time on stream i.e. 10 h. Although the Au–Fe–TiO_2 catalyst is active at low temperature (below 100 °C), we have tested the stability of the catalyst at high temperature (200, 300, 400, 500 °C, at each temperature catalyst was run continuously for 10 h). It was found that even 500 °C of reaction condition, the catalyst does not lose its activity (less than 5% catalytic activity lose), whereas Au–TiO_2 lose its activity by ca.

30%. Experiments have carried out to know the effect of reactant flow rate and moisture on the CO oxidation. The catalytic activity of Au–5Fe–TiO_2 was studied at higher flow rate of gases mixture i.e. 40 ml/min and observed 94% of CO conversion was recorded at 40 ml/min against 100% at 25 ml/min. It was also found that the catalyst is also stable to moisture. Moisture enhances the oxidation of CO, there is 100% conversion at 70 °C in presence of moisture, whereas without moisture, it shifts to 80 °C.

The promotional effect of iron on CO oxidation is due physical or textural as well as chemical (electronic) effects. Iron doping increases the specific surface area and decreases the gold particles size of the catalyst. Examination of these catalysts by X-ray photoelectron spectroscopy suggests that there are changes in the binding energy of gold. It is assumed that there may exist strong interactions between gold and Fe–TiO_2, Such interactions are also suggested by the UV–vis DRS and TPR work. Enhancement of catalytic activity by the addition of iron is due to either change in the electronic property of the catalyst or synergistic effects between gold and iron. Iron doping generated oxygen vacancies (point defects) on metal-oxide supports, which play an important role as metal cluster nucleation sites. Theoretical studies have shown that electron transfer from defects to the Au cluster facilitates CO oxidation [28,42]. Creation of new adsorption sites was observed by iron doping at Au–TiO_2 interfaces for the adsorption and activation of O_2 molecules, which assist the CO oxidation reaction. It was found that addition of iron stabilizes the particle size of gold. So there must be close contact between Au and FeO_x. The Au–FeO_x perimeter plays an important role in CO oxidation. If the reaction takes place between CO adsorbed on gold or at the Au/FeO_x perimeter and O donated by FeO_x, no migration of O and CO is required. This makes the perimeter an extremely suitable locus for reaction to take place and is associated with an increase in catalytic activity [43].

4. Conclusions

It was found that gold promoted on mesoporous Fe–TiO_2 have better activity than the neat samples towards low temperature CO oxidation reaction. Promotional effect of iron doping could be attributed to the high surface area and large porous channel in which CO and O_2 adsorption was favorable. Mean particle size of gold in the most active catalyst (Au–5Fe–TiO_2) is smaller than Au–TiO_2. We assumed that iron doping helps in creation of new adsorption sites at Au–TiO_2 interfaces for the adsorption and activation of O_2 molecules. High surface area, large porous channel, smaller gold particle, oxygen vacancies, new oxygen adsorption site and strong metal support interaction could be the reason for high catalytic activity of gold promoted Fe–TiO_2 catalyst as compared to Au–TiO_2. We observed that the gold promoted Fe–TiO_2 catalyst does not deactivate over several hours in use, even at 500 °C, whereas Au–TiO_2 loses its activity ca. 30%.

Acknowledgements

The support and permission of Prof. B.K. Mishra, Director, Institute of Minerals and Materials Technology (CSIR), Bhubaneswar is greatly acknowledged. One of the authors PM is thankful to Dr. B.K. Panda, Director, DISIR, Rajgangpur for his kind permission to carry out the collaborative work. The authors are very grateful to BRNS, Mumbai for financial support.

References

[1] M. Haruta, T. Kaboyashi, H. Sano, N. Yamada, Chem. Lett. 2 (1987) 405.
[2] M. Haruta, N. Yamada, T. Kaboyashi, S. Iijima, J. Catal. 115 (1989) 301.
[3] L. Guczi, G. Peto, A. Beck, K. Frey, O. Geszti, G. Molnar, C. Daroczi, J. Am. Chem. Soc. 125 (2003) 4332.
[4] Z. Ma, S. Brown, S.H. Overbury, S. Dai, Appl. Catal. A 327 (2007) 226.
[5] B. Solsona, M. Conte, Y. Cong, A. Carley, G. Hutchings, Chem. Commun. (2005) 2351.
[6] T. Akita, M. Okumura, K. Tanaka, S. Tsubota, M. Huruta, J. Electron Microsc. 52 (2003) 119.
[7] Z.P. Liu, S.J. Jenkins, D.A. King, Phys. Rev. Lett. 93 (2004) 156102.
[8] K. Qian, W. Huang, Z. Jiang, H. Sun, J. Catal. 248 (2007) 137.
[9] R.J. Chimentao, F. Medina, J. Fierro, J. Llorca, J.E. Sueiras, Y. Cesteros, P. Salagre, J. Mol. Catal. A 274 (2007) 159.
[10] Z. Ma, S. Overbury, S. Dai, J. Mol. Catal. A 273 (2007) 186.
[11] M.A. Debeila, R.P.K. Wells, J.A. Anderson, J. Catal. 239 (2006) 162.
[12] V. Gonzalez, R. Zanella, L. Calzada, R. Gomez, J. Phys. Chem. C 113 (2009) 8911.
[13] A. Szegedi, M. Hegedus, J.L. Margitfalvi, I. Kiricsi, Chem. Commun. (2005) 1441.
[14] T.J. Mathieson, A.G. Langdon, N.B. Milestone, B.K. Nicholson, Chem. Commun. (1998) 371.
[15] D. Cameron, R. Holliday, D. Thompson, J. Power Sources 118 (2003) 298.
[16] J.G. Carriazo, L.M. Martınez, J.A. Odriozola, S. Moreno, R. Molina, M.A. Centeno, Appl. Catal. B 72 (2007) 157.
[17] B. Qiao, Y. Deng, Appl. Catal. B 66 (2006) 241.
[18] Y. Kang, B. Wan, Catal. Today 35 (1997) 379.
[19] K. Laszlo Guczi, A. Frey, G. Beck, C.S. Peto, N. Daroczi, S. Kruse, Chenakin, Appl. Catal. A 291 (2005) 116.
[20] J.G. Carriazo, L.M. Martınez, J.A. Odriozola, S. Moreno, R. Molina, M.A. Centeno, Appl. Catal. B: Environ. 72 (2007) 157.
[21] Y. Wu, J. Zhang, L. Xiao, F. Chen, Appl. Catal. B 88 (2009) 525.
[22] M. Shou, H. Takekawa, D. Ju, T. Hagiwara, D. Lu, K. Tanaka, Catal. Lett. 108 (2006) 119.
[23] S. Carrettin, Y. Hao, V.A. Guerrero, B.C. Gates, S. Trasobares, J. Calvino, A. Corma, Chem. Eur. J. 13 (2007) 7771.
[24] S. Albonetti, R. Bonelli, J. Mengou, C. Femoni, C. Tiozzo, S. Zacchini, F. Trifiro, Catal. Today 137 (2008) 483.
[25] H. Li, X. Zhang, Y. Huo, J. Jhu, Environ. Sci. Technol. 41 (2007) 4410.
[26] W.F. Zhang, M.S. Zhang, Z. Yin, Q. Chen, Appl. Phys. B 70 (2000) 261.
[27] K.Y. Jung, S.B. Park, M. Anpo, J. Photochem. Photobiol. A 170 (2005) 247.
[28] W.T. Wallace, B.K. Min, D.W. Goodman, J. Mol. Catal. A 228 (2005) 3.
[29] M. Dewan, G. Zhang, O. Ostrovski, Metall. Mater. Trans. B 40 (2009) 62.
[30] A. Gomez-Cortes, G. Dıaz, R. Zanella, H. Ramırez, P. Santiago, J.M. Saniger, J. Phys. Chem. C 113 (2009) 9710.
[31] G.L. Haller, D.E. Resasco, Adv. Catal. 36 (1989) 173.
[32] E.P. Reddy, L. Davydov, P.G. Smirniotis, J. Phys. Chem. B 106 (2002) 3394.
[33] Z. Zhu, M. Hartmann, E.M. Maes, R.S. Czernuszewicz, L. Kevan, J. Phys. Chem. B 104 (2000) 4690.
[34] S. Minico, S. Scire, C. Crisafulli, R. Maggiore, S. Galvagno, Appl. Catal. B: Environ. 28 (2000) 245.
[35] G. Neri, A.M. Visco, S. Galvagno, A. Donato, M. Panzalorto, Thermochim. Acta 329 (1999) 39.
[36] G. Munteanu, L. Ilieva, D. Andreeva, Thermochim. Acta 291 (1997) 171.
[37] G.J. Hutchings, M. Hall, A. Carley, P. Landon, B.E. Solsona, C.J. Kiely, A. Herzing, M. Makkee, J. Moulijn, A. Overweg, J. Gonzalez, J. Guzman, B.C. Gates, J. Catal. 242 (2006) 71.
[38] F. Moreau, G.C. Bond, Catal. Today 114 (2006) 362.
[39] F. Moreau, G.C. Bond, Top. Catal. 44 (2007) 95.
[40] G. Srinivas, J. Wright, C.S. Bai, R. Cook, Proc. 11th Int. Congr. Catal Stud. Surf. Sci. Catal. 101 (1996) 427.
[41] S.T. Daniels, A.R. Overweg, M. Makkee, J.A. Moulijn, J. Catal. 230 (2005) 52.
[42] J.D. Grunwaldt, A. Baiker, J. Phys. Chem. B 103 (1999) 1002.
[43] R.J.H. Grisel, B.E. Nieuwenhuys, Catal. Today 64 (2001) 69.